CrossMark click for updates

Stoichiometry of $LaAlO_3$ films grown on $SrTiO_3$ by pulsed laser deposition

M. Golalikhani,[1,a)] Q. Y. Lei,[1] G. Chen,[2] J. E. Spanier,[2] H. Ghassemi,[2] C. L. Johnson,[2] M. L. Taheri,[2] and X. X. Xi[1]
[1]*Department of Physics, Temple University, Philadelphia, Pennsylvania 19122, USA*
[2]*Department of Materials Science & Engineering, Drexel University, Philadelphia, Pennsylvania 19104, USA*

(Received 28 December 2012; accepted 4 March 2013; published online 10 July 2013)

We have studied the stoichiometry of epitaxial $LaAlO_3$ thin films on $SrTiO_3$ substrate grown by pulsed laser deposition as a function of laser energy density and oxygen pressure during the film growth. Both x-ray diffraction (θ-2θ scan and reciprocal space mapping) and transmission electron microscopy (geometric phase analysis) revealed a change of lattice constant in the film with the distance from the substrate. Combined with composition analysis using x-ray fluorescence we found that the nominal unit-cell volume expanded when the $LaAlO_3$ film was La-rich, but remained near the bulk value when the film was La-poor or stoichiometric. La excess was found in all the films deposited in oxygen pressures lower than 10^{-2} Torr. We conclude that the discussion of $LaAlO_3/SrTiO_3$ interfacial properties should include the effects of cation off-stoichiometry in the $LaAlO_3$ films when the deposition is conducted under low oxygen pressures. © *2013 AIP Publishing LLC*. [http://dx.doi.org/10.1063/1.4811821]

I. INTRODUCTION

Since the discovery of a high-mobility conducting layer between the TiO_2-terminated $SrTiO_3$ substrate and $LaAlO_3$ thin film by Ohtomo and Hwang,[1] the origin of this 2-dimensional electron gas (2DEG) system has been intensively studied.[2] Several mechanisms have been proposed including electronic reconstruction,[1–6] oxygen vacancy effects,[6–10] defects due to laser bombardment,[11] and interfacial ion intermixing between $LaAlO_3$ and $SrTiO_3$.[3,12,13] Recently, it has been shown both theoretically[14] and experimentally[15,16] that the transport property of the interface changes drastically when the $LaAlO_3$ film stoichiometry is varied. Since most of the $LaAlO_3$ films for the 2DEG studies were grown by pulsed laser deposition (PLD) and a wide range of growth conditions in terms of laser energy density and oxygen pressure have been used, a systematic study of the $LaAlO_3$ film stoichiometry as a function of PLD growth conditions is critically needed. Only few reports exist in the literature on this issue and the scopes of these studies are limited.[17,18] In addition, although a low oxygen pressure during the film deposition can lead to oxygen vacancies in the $SrTiO_3$ substrate, which affect the measured transport property,[6–10] it could also affect the $LaAlO_3$ film stoichiometry. It is important to separate the oxygen vacancy effect from that of cation off-stoichiometry in the $LaAlO_3$ film.

Here, we present a systematic study on the laser energy density and oxygen pressure effects on the $LaAlO_3$ film stoichiometry by structural and compositional analyses. In the range of the deposition parameters we have studied, we found that the $LaAlO_3$ film stoichiometry depends strongly on the oxygen pressure during the deposition, and not significantly on the laser energy density. The optimal oxygen pressure for stoichiometric $LaAlO_3$ films is about 100 mTorr. Although the details of the result could be different for different experimental setups, our results indicate that $LaAlO_3$ film stoichiometry should be considered in the discussions of 2DEG properties at the $LaAlO_3/SrTiO_3$ interface under various deposition conditions.

[a)]Author to whom correspondence should be addressed. Electronic mail: tuc32533@temple.edu

II. EXPERIMENT

The $LaAlO_3$ thin films used in this work were grown on (001) $SrTiO_3$ substrates by PLD using a KrF excimer laser ($\lambda = 248$ nm, and pulse duration 25 ns) from a single crystal $LaAlO_3$ target. The depositions were carried out at various laser energy densities, from 0.7 to 2 J/cm^2, and oxygen pressures, between 0.3 and 10^{-4} Torr (the background vacuum is 10^{-5} to 10^{-6} Torr). The growth rate of the $LaAlO_3$ film was calibrated at the identical growth conditions prior to each growth using Dektak profilometer. The growth time was fixed at 15 min for all the films. In order to keep the total film thickness at about 100 nm repetition rate of the laser pulses was varied for each sample to accommodate the change in the growth rate, from 1.2 Hz (for laser energy density of 2 J/cm^2 and oxygen pressure of 300 mTorr) to 13.5 Hz (for laser energy density of 0.7 J/cm^2 and oxygen pressure of 10^{-2} Torr). The depositions were carried out at 730 °C substrate temperature and the samples were cooled down to room temperature after growth at an oxygen pressure of 200 Torr.

The structural properties of the deposited $LaAlO_3$ films were analyzed by x-ray diffraction (XRD) using a Bruker D8 Discover diffractometer. The film texture and epitaxial quality were characterized by θ-2θ scan, azimuthal φ scan, and reciprocal space mapping (RSM), from which the out-of-plane and in-plane lattice constants of the $LaAlO_3$ films were calculated. The uncalibrated La/Al ratios presented in this paper, were determined by x-ray fluorescence (XRF) with an iXRF^{TM} model 550 system interfaced to an FEI DB235 dual-beam scanning electron and ion beam microscope. The XRF system uses an Ag-target, an fX X-ray tube, and a

0021-8979/2013/114(2)/027008/5/$30.00 © 2013 AIP Publishing LLC

[This article is copyrighted as indicated in the abstract. Reuse of AIP content is subject to the terms at: http://scitation.aip.org/termsconditions. Downloaded to] IP: 144.118.64.194 On: Thu, 28 Nov 2013 02:17:19

liquid nitrogen-cooled SiLi detector. The x-ray source produces a collimated 500-μm beam spot on the sample. Quantitative analysis was performed using the EDS2008 software. Using high-resolution transmission electron microscopy (HRTEM) images, geometric phase analysis (GPA)[19,20] was carried out to quantify the strain as a function of distance from the interface. Cross section samples were prepared via an *in situ* lift-out process using an FEI Strata DB235 focused ion beam (FIB) system,[21] and then analyzed using a JEOL JEM2100 TEM operated at 200 kV.

III. RESULTS AND DISCUSSIONS

The PLD-deposited $LaAlO_3$ thin films grow epitaxially on the (001) $SrTiO_3$ substrates. Figure 1 shows (a) a θ-2θ scan and (b) an azimuthal φ scan of the (103) diffraction peak for a $LaAlO_3$ film deposited with a laser energy density of 1.5 J/cm^2 in an oxygen pressure of 100 mTorr. Besides the substrate peaks, only (00*L*) diffractions from the film are present in the θ-2θ scan, indicating that the *c*-axis of the film is oriented normal to the substrate surface. A Nelson-Riley fitting of the diffraction peaks gives a *c*-axis lattice constant of 3.78 ± 0.01 Å for the film. The lattice constant can also be calculated using the $SrTiO_3$ peak as a reference ($a = 3.905$ Å). The *c*-axis lattice constant thus calculated is 3.78 ± 0.01 Å, consistent with the Nelson-Riley fitting. Figure 1(b) shows φ scans for both the $LaAlO_3$ film and the $SrTiO_3$ substrate. Both scans show a four-fold symmetry and the film and substrate peaks overlap, suggesting a cube-on-cube epitaxial relationship LAO (100) [001]//STO (100) [001]. From the φ scan the *a*-axis lattice constant of the film is calculated to be 3.82 ± 0.02 Å, a tensile strain of 0.7% from the bulk value of 3.789 Å. The result indicates that the epitaxial strain in the 100 nm-thick $LaAlO_3$ film is mostly relaxed. The volume of the pseudo-cubic unit cell of the film is 54.988 Å^3, a 1% expansion compared to the bulk value of 54.397 Å^3. The epitaxial growth shown by Fig. 1 is typical of all the films in this work except that the lattice constants are different for films deposited under different conditions.

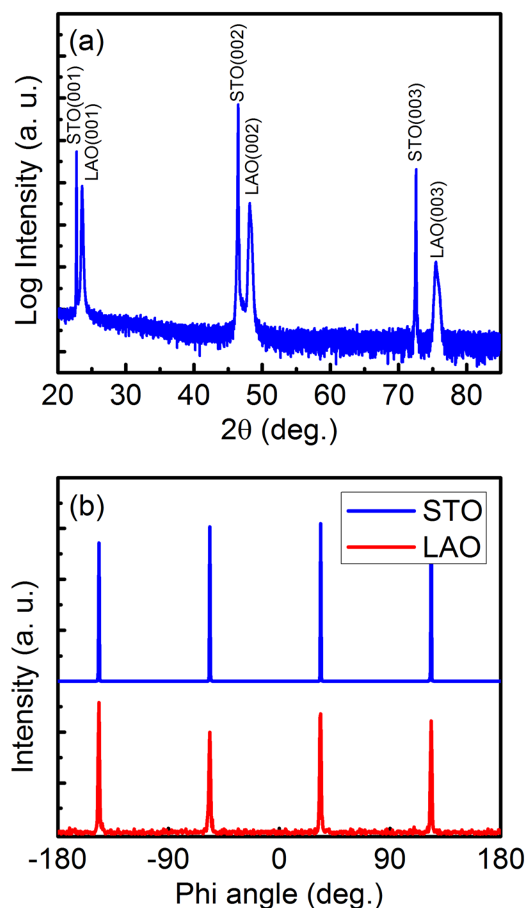

FIG. 1. Typical XRD spectra for a $LaAlO_3$ film. (a) A θ-2θ scan. (b) Azimuthal φ scans of the (103) peaks of the $LaAlO_3$ film and the $SrTiO_3$ substrate.

The uncalibrated cation stoichiometry of the $LaAlO_3$ film in Fig. 1 was measured by XRF. Because the x-ray source for XRF is brighter than the electron beam often used in energy dispersive spectroscopy (EDS), XRF provides higher sensitivity for the elemental analysis of surfaces and thin films. In the XRF spectrum in Fig. 2, emission peaks of the characteristic secondary x-rays from La and Al in the film and Sr and Ti from the substrate are seen. The peaks were fitted with Gaussian distributions, which effectively resolved the overlap of, for example, the Ti K_α and La L_α peaks. The relative areas under the Gaussian peaks of La and Al, with the ZAF correction, were used to obtain the La/Al cation ratio, *x*. The K_α peak of Al and the L_α peak of La were chosen for all the XRF analysis in this work, although the use of the L_β and L_γ peaks of La provided similar results. For the film shown in the figure, the uncalibrated La/Al cation ratio from the XRF analysis is 0.91 ± 0.03.

$LaAlO_3$ films deposited under different conditions were characterized by both the XRD and the XRF measurements. The laser energy densities used were 0.7, 1.0, 1.5, and 2.0 J/cm^2, and the oxygen pressures used were 1×10^{-4}, 1×10^{-3}, 1×10^{-2}, 1×10^{-1}, and 3×10^{-4} Torr. Since both laser energy density and oxygen pressure can affect the result, all combinations of the two parameters were studied. Figure 3 shows the XRD results for three representative films deposited with different laser energy densities and oxygen pressures, resulting in different La/Al cation ratios: (a) and (d) 0.7 J/cm^2, 300 mTorr, and $x = 0.62$; (b) and (e) 1 J/cm^2, 100 mTorr, and $x = 1.01$; and (c) and (f) 1 J/cm^2, 10^{-4} Torr, and $x = 1.19$. Figures 3(a)–3(c) are θ-2θ profiles around the (002) $SrTiO_3$ Bragg reflection (the dashed lines represent the bulk *c*-axis lattice constant of

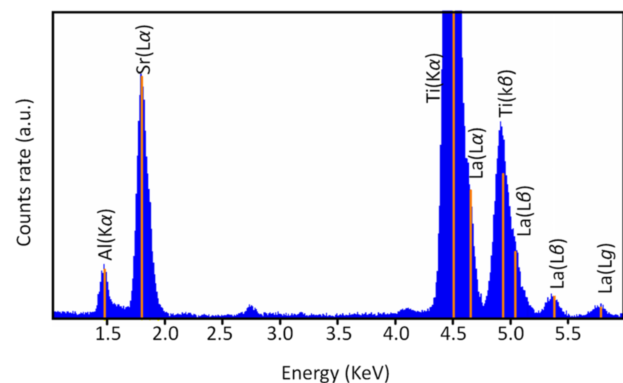

FIG. 2. XRF spectrum for the $LaAlO_3$ film shown in Fig. 1.

[This article is copyrighted as indicated in the abstract. Reuse of AIP content is subject to the terms at: http://scitation.aip.org/termsconditions. Downloaded to] IP: 144.118.64.194 On: Thu, 28 Nov 2013 02:17:19

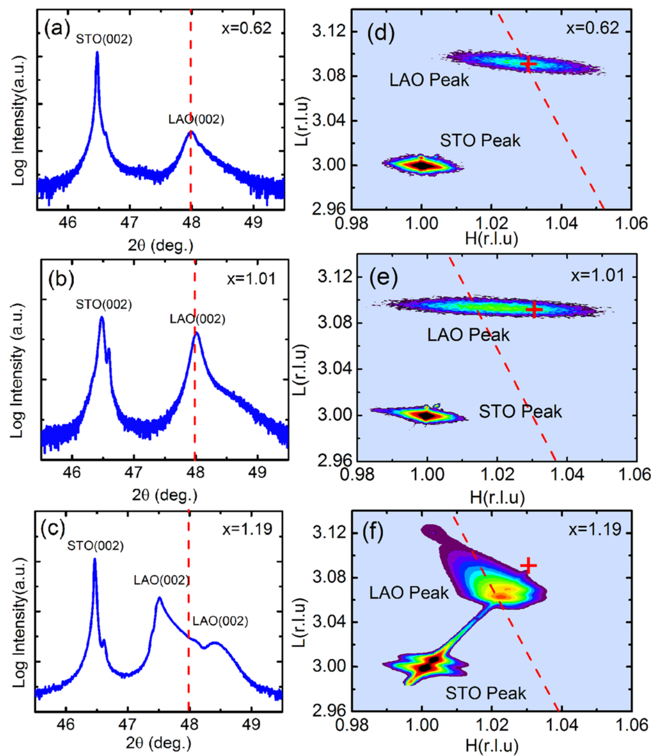

FIG. 3. XRD spectra for $LaAlO_3$ films with different x = La/Al cation ratios deposited with different laser energy densities and oxygen pressures: (a) and (d) 0.7 J/cm^2 and 300 mTorr; (b) and (e) 1 J/cm^2 and 100 mTorr; and (c) and (f) 1 J/cm^2 and 10^{-4} Torr. Figures (a)–(c) are θ-2θ profiles around the (002) $SrTiO_3$ peak and (d)–(f) are logarithmic RSM contour plots around the (103) $SrTiO_3$ spot. The dashed lines in (a)–(c) and the red "+" signs in (d)–(f) correspond to the values of bulk $LaAlO_3$. The dashed lines in (d)–(f) are points in the reciprocal space with equal unit-cell volumes.

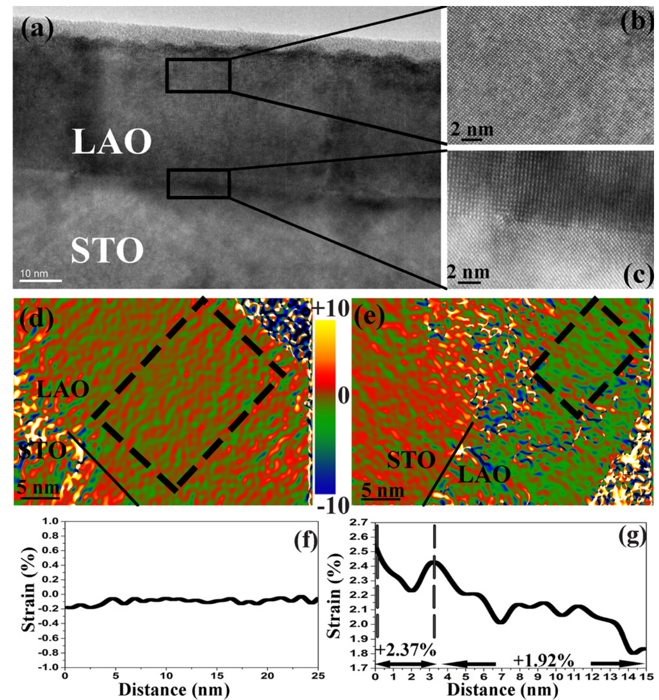

FIG. 4. HRTEM images and in-plane map of strain in parallel to the interface direction for the film in Fig. 1. (a) A low-magnification TEM image. (b) and (c) HRTEM images of the top part of the $LaAlO_3$ layer and its interface with $SrTiO_3$, respectively. (d) and (e) GPA strain analysis of the edge of the $LaAlO_3$ layer and the $LaAlO_3/SrTiO_3$ interface, respectively. The dotted boxes indicate the regions which were used to measure the average strain. (f) Average strain gradients inside the dotted boxes shown in (d), where the x-axis ends at the edge of the $LaAlO_3$ layer. (g) Average strain gradients inside the dotted boxes shown in (e), where the x-axis starts at the $LaAlO_3/SrTiO_3$ interface.

$LaAlO_3$). Figures 3(d)–3(f) are reciprocal space maps around the (103) peak of the $SrTiO_3$ substrate (the red "+" symbols correspond to the reciprocal point of bulk $LaAlO_3$). The θ-2θ scans show broader film peaks than the substrate peak, in particular for the La-rich film, which displays a clear double-peak structure. This is confirmed by the RSM maps showing broadening of the film spots in the L direction, suggesting that the out-of-plane c-axis lattice constants of the films are not uniform across the film thickness. The peak values suggest c-axis lattice constants similar to that of the bulk $LaAlO_3$ for the La-poor and stoichiometric films and larger than the bulk value for the La-rich film. The non-uniformity is more severe in the a-axis lattice constant. From the RSM maps one can see significant broadening of the film spots in the H direction, with the overall in-plane a-axis lattice constants larger than that of the bulk $LaAlO_3$ in the near stoichiometric and La-rich films.

The broadenings of the diffraction peaks in the θ-2θ scans and RSM contour maps are the result of strain relaxation in the epitaxially grown $LaAlO_3$ film, which experiences a tensile stress of 3% on the $SrTiO_3$ substrate. Above a critical thickness, which depends on the deposition conditions and is around 4 nm, the strain in the $LaAlO_3$ film starts to relax. This is revealed by the result of geometric phase analysis (shown in Fig. 4), which was performed on the $LaAlO_3$ film in Fig. 1.

Figure 4 illustrates the changing of strain in the $LaAlO_3$ film relative to its interface with the $SrTiO_3$ substrate. Figure 4(a) is a low-magnification TEM image of the $LaAlO_3$ film on top of the $SrTiO_3$ substrate, showing a film thickness of ~100 nm. From Figs. 4(b) and 4(c), which illustrate HRTEM images of the top part of the $LaAlO_3$ layer and its interface with $SrTiO_3$, respectively, one can see more contrast, indicating more strain, near the $LaAlO_3/SrTiO_3$ interface. The region indicated with the dotted box in Fig. 4(d) and the average strain profile shown in Fig. 4(f) represent insignificant strain gradient on top of the $LaAlO_3$ layer, which confirms its relaxation away from the interface. The average strain values on top of the $LaAlO_3$ layer was measured ~−0.06%, which is below the 0.1% resolution of the GPA technique. The dotted box covers the top 25 nm [x-axis in Fig. 4(f)] of the $LaAlO_3$ layer; therefore, the x-axis ends at the edge of the $LaAlO_3$ layer. Figures 4(e) and 4(g) illustrate the profile of the strain starting at the $LaAlO_3/SrTiO_3$ interface into the $LaAlO_3$ layer [x-axis in Fig. 4(g)]. The strain profile indicates that at the first ~4 nm distance from the interface, the $LaAlO_3$ layer is under an average tensile strain of 2.37% compared to the bulk $LaAlO_3$, which decreases to 1.7% after ~15 nm from the interface. These results confirm the existence of strain gradient in the $LaAlO_3$ layer as a function of the distance from the interface toward the film surface.

The result in Fig. 3 indicates that the strain relaxation depends on the compositions of the $LaAlO_3$ films. The

[This article is copyrighted as indicated in the abstract. Reuse of AIP content is subject to the terms at: http://scitation.aip.org/termsconditions. Downloaded to] IP: 144.118.64.194 On: Thu, 28 Nov 2013 02:17:19

relaxation is the most gradual in the near stoichiometric film—the in-plane lattice constant ranges from that of the $SrTiO_3$ substrate to that of the bulk $LaAlO_3$. For the La-poor film, the relaxation occurs the fastest—the coherently strained layer is too thin to be detectable by RSM and the *a*-axis lattice constant of the film is close to the bulk value. In the La-rich film, both the in-plane and the out-of-plane lattice constants vary substantially across the film thickness, with both *a*- and *c*-axis lattice constants larger than those of the bulk $LaAlO_3$.

Ohnishi *et al*. have shown that lattice expansion often observed in homoepitaxial $SrTiO_3$ films is not due to oxygen vacancies but originates from cation off-stoichiometry.[22] Thus, the lattice expansion in homoepitaxial $SrTiO_3$ films has been used as a sensitive indicator of cation off-stoichiometry.[22–25] Since there is no epitaxial strain in the homoepitaxial $SrTiO_3$ film on $SrTiO_3$ substrate, the increased *c*-axis lattice constant alone can represent the lattice expansion. The strain and strain relaxation in the $LaAlO_3$ films on $SrTiO_3$ make the task of correlating lattice expansion to film stoichiometry much more complex as the lattice constants vary continuously across the film thickness. Assuming that the film composition does not change throughout a film, we draw lines of equal unit-cell volume on the RSM maps and take the peak intensity values [the dashed lines shown in Figs. 3(d)–3(f)] as the nominal unit-cell volumes of the films. The two equal-volume lines passing through the half maximum intensity define the error bar. In Fig. 5, the unit-cell volume versus the La/Al cation ratio is plotted for 20 $LaAlO_3$ films fabricated under different conditions. The $LaAlO_3$ bulk value is shown as a dashed line. Despite the large error bars in the volume, a trend is evident: The unit-cell volume increases from the bulk value when the film is increasingly La-rich, reaching about 4%; for La-poor and stoichiometric films, the volume expansion is not as severe and the unit-cell volume is similar to that of the bulk $LaAlO_3$. While we cannot rule out the effect of oxygen vacancies on the volume expansion in the $LaAlO_3$ films, the result clearly shows the correlation between the cation stoichiometry and the lattice expansion. Even with the complications due to strain and strain relaxation in the $LaAlO_3$ film, one can use the unit-cell volume as an indication of the film stoichiometry similar to the case of homoepitaxial $SrTiO_3$ films. In particular, when there is excess of La in the $LaAlO_3$ film the lattice expands. It is, however, not effective for detecting La deficiency in the film.

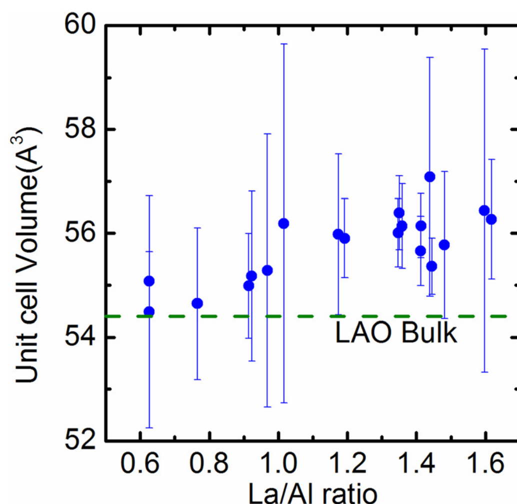

FIG. 5. Unit-cell volume of the $LaAlO_3$ films as a function of the La/Al cation ratio.

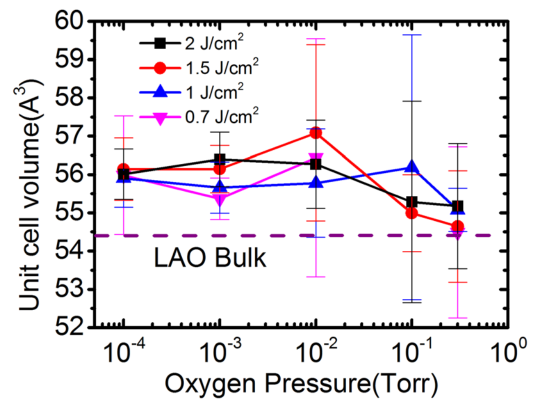

FIG. 6. Unit-cell volume of the $LaAlO_3$ films as a function of oxygen pressure during deposition for different laser energy densities.

Having established the correlation between the La/Al ratio and the nominal unit-cell volume of the $LaAlO_3$ films, we plot in Fig. 6 the unit-cell volume as a function of the oxygen pressure during the deposition for different laser energy densities. Even with the large error bars, one can see that the unit-cell volume is larger than the bulk value when the oxygen pressure is 10^{-2} Torr and lower for all the laser energy densities used for the deposition. When the oxygen pressure is 10^{-1} Torr or higher, the unit-cell volume becomes closer to that of the bulk $LaAlO_3$. In Fig. 7, the cation ratio of the film as measured by XRF is plotted as a function of oxygen pressure for different laser energy densities. For the films grown under the same oxygen pressure, no significant difference was observed in composition for different laser energy densities. For the lower oxygen pressures, 10^{-2} Torr and lower, the cation ratio exhibits a large deviation from the stoichiometry, an excess of La by as much as over 50%. As the oxygen pressure is increased to 0.1 Torr, the deviation in the La/Al ratio becomes smaller and near stoichiometric. Further increase in the oxygen pressure resulted in La

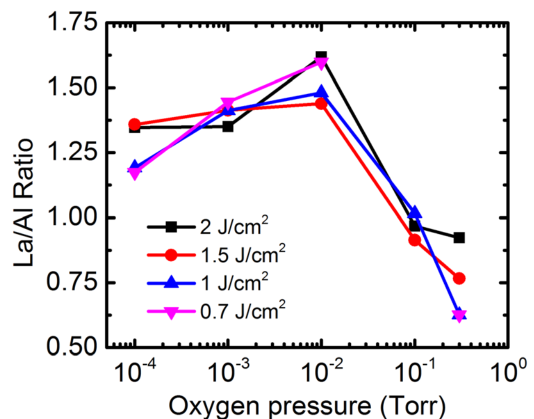

FIG. 7. The La/Al cation ratio as a function of oxygen pressure for different laser energy densities.

[This article is copyrighted as indicated in the abstract. Reuse of AIP content is subject to the terms at: http://scitation.aip.org/termsconditions. Downloaded to] IP: 144.118.64.194 On: Thu, 28 Nov 2013 02:17:19

deficiency, which cannot be detected effectively by the unit-cell volume.

The result presented here shows that the composition of the PLD deposited $LaAlO_3$ films depends on the deposition conditions. When the oxygen pressure during the deposition is lower than 10^{-2} Torr, the film becomes La-rich. The optimal oxygen pressure for film stoichiometry is about 10^{-1} Torr. Our result may have significant implications for the study of the 2DEG at the $LaAlO_3/SrTiO_3$ interfaces. As most of the reported studies of the $LaAlO_3/SrTiO_3$ interfacial properties used $LaAlO_3$ films deposited at 10^{-2} Torr oxygen pressure or lower, these films may be La-rich, which will have an influence on the properties of the 2DEG. We should point out that the La/Al ratios reported here are the nominal values obtained from 100 nm-thick $LaAlO_3$ films that have undergone various degrees of strain relaxation. It may or may not represent the film stoichiometry in the ultrathin $LaAlO_3$ layers used in the 2DEG studies. Further, the correlation between the deposition conditions and the film stoichiometry can be different for different deposition systems. Nevertheless, our result demonstrates that one needs to take into account the $LaAlO_3$ film stoichiometry, in addition to the oxygen vacancy effects, when studying the 2DEG properties at the $LaAlO_3/SrTiO_3$ interfaces using $LaAlO_3$ films deposited under low oxygen pressures.

IV. CONCLUSIONS

We present here the results of structural and composition characterizations of a series of 20 epitaxial $LaAlO_3$ films grown by PLD under different conditions. Despite the strain and strain relaxation in the $LaAlO_3$ films, we found that the unit-cell volume expands by as much as 4% when the film composition is La rich. The cation off-stoichiometry reaches over 50% La rich when the oxygen pressure during the deposition is 10^{-2} Torr or lower. No significant effect on the composition by changing the laser energy density was observed. We conclude that the $LaAlO_3$ film stoichiometry is an important factor in the 2DEG properties at the $LaAlO_3/SrTiO_3$ interface when the $LaAlO_3$ film is deposited under low oxygen pressures.

Note added in proof. After the acceptance of the paper, we became aware of the paper by E. Breckenfeld *et al.*[26] on the effects of $LaAlO_3$ stoichiometry on the transport properties of the $LaAlO_3/SrTiO_3$ interfaces. Their result clearly demonstrate the importance of the deposition conditions of the $LaAlO_3$ layer on the 2-dimensional electron gas (2DEG) system properties.

ACKNOWLEDGMENTS

The work at Temple was supported by NSF under Grant No. DMR-1245000 (M.G. and X.X.X.) and by DOE under Grant No. DE-SC0004764 (Q. Y. L. and X. X. X.). J.E.S. and G.C. acknowledge supports from NSF under Grant Nos. DMR-1124696 and DMR-0722845, and access to instrumentation in the Centralized Research Facility at Drexel. M.L.T and H.G. acknowledge support from ONR under Contract No. ONR-N00014-11-1-0296.

[1]A. Ohtomo and H. Hwang, Nature **427**, 423 (2004).
[2]P. Zubko, S. Gariglio, M. Gabay, P. Ghosez, and J. Triscone, Annu. Rev. Condens. Mater. Phys. **2**, 141 (2011).
[3]N. Nakagawa, H. Hwang, and D. Muller, Nature Mater. **5**, 204 (2006).
[4]R. Pentcheva and A. E. Pickett, J. Phys.: Condens. Matter **22**, 043001 (2010).
[5]A. D. Caviglia, S. Gariglio, C. Cancellieri, B. Sacepe, A. Fete, N. Reyren, M. Gabay, A. F. Morpurgo, and J. Triscone, Phys. Rev. Lett. **105**, 236802 (2010).
[6]M. Huijben, A. Brinkman, G. Koster, G. Rijnders, H. Hilgenkamp, and D. H. A. Blank, Adv. Mater. **21**, 1665 (2009).
[7]J. N. Eckstein, Nature Mater. **6**, 473 (2007).
[8]A. Kalabukhov, R. Gunnarsson, J. Borjesson, E. Olsson, T. Claeson, and D. Winkler, Phys. Rev. B **75**, 121404 (2007).
[9]M. Basletic, J.-L. Maurice, C. Carretero, G. Herranz, O. Copie, M. Bibes, E. Jacquet, K. Bouzehouane, S. Fusil, and A. Barthelemy, Nature Mater. **7**, 621 (2008).
[10]G. Herranz, M. Basletic, O. Copie, M. Bibes, A. N. Khodan, C. Carretero, E. Tafra, E. Jacquet, K. Bouzehouane, A. Hamzic, and A. Barthelemy, Appl. Phys. Lett. **94**, 012113 (2009).
[11]K. Shibuya, T. Ohnishi, M. Lippmaa, and M. Oshima, Appl. Phys. Lett. **91**, 232106 (2007).
[12]S. Thiel, G. Hammerl, A. Schmehl, C. W. Schneider, and J. Mannhart, Science **313**, 1942 (2006).
[13]P. R. Willmott, S. A. Pauli, R. Herger, C. M. Schlepuetz, D. Martoccia, B. D. Patterson, B. Delley, R. Clarke, D. Kumah, C. Cionca, and Y. Yacoby, Phys. Rev. Lett. **99**, 155502 (2007).
[14]A. Sorokine, D. Bocharov, S. Piskunov, and V. Kashcheyevs, Phys. Rev. B **86**, 155410 (2012).
[15]F. Schoofs, T. Fix, A. S. Kalabukhov, D. Winkler, Y. Boikov, I. Serenkov, V. Sakharov, T. Claeson, L. MacManus-Driscoll, and M. G. Blamire, J. Phys.: Condens. Matter **23**, 305002 (2011).
[16]M. Warusawithana, C. Brooks, D. Schlom, S. Thiel, J. Mannhart, N. Reyren, A. Caviglia, S. Gariglio, and J. M. Triscone, Bull. Am. Phys. Soc. **54**, BAPS.2009.MAR.Y30.4 (2009), available at http://meetings.aps.org/link/BAPS.2009.MAR.Y30.4.
[17]T. C. Droubay, L. Qiao, T. C. Kaspar, M. H. Engelhard, V. Shutthanandan, and S. A. Chambers, Appl. Phys. Lett. **97**, 124105 (2010).
[18]L. Qiao, T. C. Droubay, T. Varga, M. E. Bowden, V. Shutthanandan, Z. Zhu, T. C. Kaspar, and S. A. Chambers, Phys. Rev. B **83**, 085408 (2011).
[19]M. J. Hytch, E. Snoeck, and R. Kilaas, Ultramicroscopy **74**, 131 (1998).
[20]M. J. Hytch, J. L. Putaux, and J. M. Penisson, Nature **423**, 270 (2003).
[21]R. Wirth, Chem. Geol. **261**, 217 (2009).
[22]T. Ohnishi, K. Shibuya, T. Yamamoto, and M. Lippmaa, J. Appl. Phys. **103**, 103703 (2008).
[23]C. M. Brooks, L. F. Kourkoutis, T. Heeg, J. Schubert, D. A. Muller, and D. G. Schlom, Appl. Phys. Lett. **94**, 162905 (2009).
[24]J. M. LeBeau, R. Engel-Herbert, B. Jalan, J. Cagnon, P. Moetakef, S. Stemmer, and G. B. Stephenson, Appl. Phys. Lett. **95**, 142905 (2009).
[25]G. Z. Liu, Q. Y. Lei, and X. X. Xi, Appl. Phys. Lett. **100**, 202902 (2012).
[26]E. Breckenfeld, N. Bronn, J. Karthik, A. R. Damodaran, S. Lee, N. Mason, and L. W. Martin, Phys. Rev. Lett. **110**, 196804 (2013).

[This article is copyrighted as indicated in the abstract. Reuse of AIP content is subject to the terms at: http://scitation.aip.org/termsconditions. Downloaded to] IP: 144.118.64.194 On: Thu, 28 Nov 2013 02:17:19